An algorithm for the choice of the regularization parameter in inverse problems in imaging

E. Loli Piccolomini* F. Zama†

August 1, 2011

Abstract

In this paper we present an iterative algorithm for the solution of regularization problems arising in inverse image processing. The regularization function to be minimized is constituted by two terms, a data fit function and a regularization function, weighted by a regularization parameter. The proposed algorithm solves the minimization problem and estimates the regularization parameter by an iterative procedure. Numerical results on image denoising, deblurring and tomographic images reconstruction show that the method is efficient and computationally fast in these applications.

Keywords: Inverse imaging problems, Constrained optimization, Iterative methods.
Classification: 65R30, 65R32, 65F22.

1 Introduction

Many inverse problems in imaging arise from the discretization of a first kind Fredholm integral equation:

$$g(x,y) = \int_\Omega K(x,y,\xi,\eta) f(\xi,\eta) d\xi d\eta \tag{1}$$

where Ω is the image domain, f is the image function, g is the data function and K is the operator describing the image formation process. For example, in image deblurring K is the Point Spread Function (PSF), in tomographic imaging (TAC, SPECT, PET) K is the Radon operator, in Magnetic Resonance Imaging K is the complex exponential function of the Fourier Transform. The discretization of (1) leads to the linear system:

$$K\mathbf{f} = \mathbf{g}. \tag{2}$$

*Department of Mathematics, University of Bologna, e-mail: piccolom@dm.unibo.it
†Department of Mathematics, University of Bologna, e-mail: zama@dm.unibo.it

If the data $\mathbf{g}$ are contaminated by noise, the least-squares solution of (2) is dominated by noise, because of the ill-posed nature of problem (1). A regularization method is needed to compute a good solution of (2). A common approach is to solve a minimization problem of the form [11]:

$$minJ(\mathbf{f}) = \|K\mathbf{f} - \mathbf{g}\|^2 + \lambda(\mathcal{R}(\mathbf{f}) - \gamma) \tag{3}$$

where $R(f)$ is the regularization function, λ is the regularization parameter and γ represents the smoothness level required in the solution. A reference value for γ is given by is an estimate of $\mathcal{R}(\mathbf{f}^*)$, where $\mathbf{f}^*$ is the regularized solution. Since this value is unknown γ is defined heuristically or using some given a priori information. The function $\mathcal{R}(\mathbf{f})$ describes the kind of regularity required on the solution and its choice usually depends on the characteristics both of the image and application considered.

Finding a good value of λ is a challenging in this framework. When white noise is added to the data, an optimal value of λ cannot be found without knowing the variance of the noise (Bakushinki's Theorem [4]). However, in imaging applications the variance of the noise is usually unknown; moreover, it is sufficient to have a good approximation of the optimal value of the regularization parameter. For this reason, different heuristic rules have been proposed in literature to compute a suitable value of λ in inverse imaging applications with unknown variance of the noise for different regularization functions $\mathcal{R}(\mathbf{f})$. In [1] we proposed the `CLSRit` method, an iterative method that finds a regularized solution $\mathbf{f}$ and computing a suitable value of λ and γ. In [1] we tested the method on one dimensional problems from Hansen's RegTool package [7] with $\mathcal{R}(\cdot) = \|\cdot\|_p^p$, $1 < p < \infty$. Aim of this paper is to show the effectiveness of the method in inverse imaging applications, extending it to other regularization functions $\mathcal{R}(\mathbf{f})$ such as Total Variation (TV) function [10, 12].

Numerical methods using expensive matrix factorizations cannot be efficiently applied to imaging applications. Moreover, the proposed method is computationally very efficient and it is easily extensible to other regularization functions $\mathcal{R}(\mathbf{f})$ and to general nonlinear fit-to-data functions different from the least-squares, such as the Csiszàr I-divergence [2].

The paper is organized as follows. In section 2 the Constrained Least Squares Regularization `CLSRit` algorithm applied to inverse imaging is illustrated and in section 3 some numerical tests on different imaging applications are reported. Finally, the conclusions are reported in section 4.

2 The method

In this section we briefly describe the `CLSRit` method and its applications to inverse imaging referring to [1] for the convergence properties.

Under the assumption that $\mathcal{R}(\cdot)$ is continuously differentiable and convex function, the problem (3) has a unique solution $\forall\lambda$ s.t. $0 < \lambda < \infty$ and for any given value $\gamma > 0$. If we fix γ and consider λ as a parameter to be determined

in (3), then the function:

$$\mathcal{L}(\mathbf{f},\lambda) \equiv \|\mathbf{K}\mathbf{f}-\mathbf{g}\|^2 + \lambda\left(\mathcal{R}(\mathbf{f})-\gamma\right) \tag{4}$$

is the Lagrangian function of the constrained minimization problem:

$$\min_{\mathbf{f}} \|\mathbf{K}\mathbf{f}-\mathbf{g}\|^2 : \ s.t. \quad \mathcal{R}(\mathbf{f}) \leq \gamma, \quad \gamma > 0 \tag{5}$$

The value $\hat{\lambda}$ representing the Lagrange multiplier of (5) produces a solution $\hat{\mathbf{f}}$ of (3) satisfying the prescribed regularity condition $\mathcal{R}(\hat{\mathbf{f}}) \leq \gamma$.

Using the constrained formulation (5) in place of (3) in imaging applications is advantageous because it is easier to estimate γ than the regularization parameter λ. Actually a good value for γ can be inferred by the physical system considered. In this paper, we propose a way for estimating γ in the case of some inverse imaging applications, such as deblurring and denoisig or tomographic reconstruction.

For the solution of problem (5), we consider the equivalent dual formulation:

$$\max_{\lambda} \Phi(\lambda) \tag{6}$$

where

$$\Phi(\lambda) = min_{\mathbf{f}}\mathcal{L}(\mathbf{f},\lambda) = min_{\mathbf{f}}\|\mathbf{K}\mathbf{f}-\mathbf{g}\|^2 + \lambda(\mathcal{R}(\mathbf{f})-\gamma).$$

In this way, the problem (5) can be separately solved for λ and $\mathbf{f}$.

For the convexity hypothesis on $\mathcal{R}$, the solution $\hat{\lambda}$ of (6) can be computed by imposing the first order conditions $\nabla_\lambda \mathcal{L}(\lambda) = 0$ i.e.

$$\nabla_\lambda \mathcal{L}(\lambda) = \nabla_\lambda \mathbf{f}(\lambda)\nabla_f \mathcal{L}(\mathbf{f}(\lambda),\lambda) + \nabla_\lambda \mathcal{L}(\mathbf{f}(\lambda),\lambda) = \nabla_\lambda \mathcal{L}(\mathbf{f}(\lambda),\lambda) = \mathcal{R}(\mathbf{f}(\lambda)) - \gamma = 0.$$

Hence, the solution of (6) can be computed as follows:

$$\begin{gathered} find \ \ \lambda \ \ s.t.\ G(\lambda) = \mathcal{R}(\mathbf{f}(\lambda)) - \gamma = 0 \ \ with\ \mathbf{f}(\lambda) \ \ s.t. \\ \mathbf{K}^T\mathbf{K}\mathbf{f}(\lambda) + \lambda\nabla_f \mathcal{R}(\mathbf{f}(\lambda)) - \mathbf{K}^T\mathbf{g} = 0 \end{gathered} \tag{7}$$

In [1] (Proposition 1) we showed that, under suitable hypotheses on λ_0 and $\mathcal{R}(\mathbf{f}(\lambda))$, the nonlinear equation

$$\mathcal{R}(\mathbf{f}(\lambda)) - \gamma = 0 \tag{8}$$

can be solved by an iterative method computing a sequence $\{\lambda_k\}$ that converges to the lagrance multiplier $\hat{\lambda}$. In particular, given λ_0 as starting value, using the bisection method we have:

$$\lambda_k = \mathcal{F}_b(\lambda_{k-1}), \quad \mathcal{F}_b(\lambda_{k-1}) = \lambda_{k-1} + sign(\mathcal{R}(\mathbf{f}(\lambda_{k-1}) - \gamma)\frac{\lambda_0}{2^k}, \quad k = 1, 2\ldots \tag{9}$$

and given λ_0,and λ_1 as starting values using the secant method we have:

$$\lambda_k = \mathcal{F}_s(\lambda_{k-1}), \quad \mathcal{F}_s(\lambda_{k-1}) = \lambda_{k-1} - \frac{\mathcal{R}(\mathbf{f}(\lambda_{k-1})) - \gamma}{\mathcal{R}(\mathbf{f}(\lambda_{k-1})) - \mathcal{R}(\mathbf{f}(\lambda_{k-2}))}\left(\lambda_{k-1} - \lambda_{k-2}\right), \quad k \geq 2\ldots \tag{10}$$

In this paper we use an hybrid method using first some bisection iterations and later some secant iterations.

The algorithm is sketched in table 1 where k_s is the number of bisection iterations to be performed in the hybrid method before starting the secant iterations. The exit condition to stop the algorithm is the following:

$$|G(\lambda_k)| < \tau_r |G(\lambda_0)| + \tau_a \quad \text{or} \quad |\lambda_k - \lambda_{k-1}| < \tau \quad \text{or} \quad k > maxit. \tag{11}$$

where τ_a, τ_r are relative and absolute tolerance parameters, τ represents the prescribed absolute tolerance of the result and $G(\lambda)$ is defined in (7).

Algorithm 1 (`CLSRit`($\mathbf{K}$, $\mathbf{g}$,γ, k_s)).
set $k = 0$
`repeat`
$k = k + 1$
`if` $k < k_s$
$\lambda_k = \mathcal{F}_b(\lambda_{k-1})$ *as in* (9)
`else`
$\lambda_k = \mathcal{F}_s(\lambda_{k-1})$ *as in* (10)
`end`
`compute` $\mathbf{f}(\lambda_k)$ *solving*
$\mathbf{K}^t\mathbf{K}\mathbf{f}(\lambda_k) + \lambda_k \nabla_x \mathcal{R}(\mathbf{f}(\lambda_k)) - \mathbf{K}^t\mathbf{g} = 0$
`until` *exit condition* (11)

Table 1: Algorithm `CLSRit`.

The parameter γ is chosen as an intermediate value in the interval $[\gamma_L, \gamma_H]$ in (3) and is computed as follows:

$$\gamma = \theta\gamma_L + (1-\theta)\gamma_H, \quad 0 \le \theta \le 1 \tag{12}$$

where $\gamma_L \equiv \mathcal{R}(\mathbf{f}_L)$ and $\mathbf{f}_L$ is an oversmoothed solution suitably computed in each application and $\gamma_H > \gamma_L$. More details on the choice of γ_H and γ_L are reported in section 3.

The more expensive computation step of the algorithm is the solution of the linear or nonlinear systems of equations:

$$\mathbf{K}^T\mathbf{K}\mathbf{f}(\lambda_k) + \lambda_k \nabla_x \mathcal{R}(\mathbf{f}(\lambda_k)) - \mathbf{K}^T\mathbf{g} = 0.$$

Different methods can be used depending both on the function $\mathcal{R}$ and on the properties of the matrix $\mathbf{K}$. In this paper we consider some choices of $\mathcal{R}$ and $\mathbf{K}$ arising in particular imaging applications: denosing, deblurring and tomographic images reconstruction.

1. $\mathcal{R}(\mathbf{f}) = TV(\mathbf{f})$. The Total Variation function.
The Total Variation function applied on a $m \times n$ image is defined as:

$$\mathcal{R}(\mathbf{f}) = \frac{1}{mn} \sum_{i=1}^{m} \sum_{j=1}^{n} \sqrt{|\nabla \mathbf{f}_{i,j}|^2 + \beta} \tag{13}$$

where ∇ is the discrete gradient operator and β is a small positive parameter usually introduced to overcome the nondifferentiability of the Euclidean norm [12, 13]. In our tests on different application problems the value $\beta = 1.e-2$ has been used.
In this case the nonlinear system (7) is solved by considering the equivalent convex minimization problem:

$$min_f \|\mathbf{K}\mathbf{f}(\lambda_k) - \mathbf{g}\|_2^2 + \lambda_k TV(\mathbf{f}(\lambda_k)). \tag{14}$$

Several methods have been proposed in literature for the solution of problem (14). The classical fixed-point method proposed by Vogel [13] has a rather slow convergence but it is very robust. Another efficient algorithm is the TWIST algorithm of Bioucas-Dias [3]. An exhaustive list of methods with available software can be found in [8]. Some of the cited methods are designed only for the denoising applications, where $\mathbf{K} = I$; others can be applied even in the deblurring case, where $\mathbf{K} \neq I$. The TWIST algorithm is an iterative shrinkage/thresholding method and it is more general than the others, since it can be applied to a general convex optimization problem of the form (3). For example, in image restoration, other suitable regularization functions are the weighted L^P norms:

$$\mathcal{R}(\mathbf{f}) = \|\mathbf{f}\|_{P,W} = \big(\sum_i w_i |\mathbf{f}_i|^p\big)^{1/p}, \quad W = (w_1, \ldots, w_{nm}), \quad w_i > 0.$$

2. $\mathcal{R}(\mathbf{f}) = \|\mathbf{L}\mathbf{f}\|_2^2$. Tikhonov regularization function.
In this case $\mathbf{L}$ is the identity matrix or the discretization of the Laplacian operator. We compute an approximate discrete Laplacian of the $n \times m$ image $\mathbf{f}$ as follows:

$$L = I_n \otimes D_{2,m} + D_{2,n} \otimes I_m$$

where I_n, I_m are the identity matrices of order n and m and $D_{2,n}$, $D_{2,m}$ are respectively $n \times n$ and $m \times m$ tridiagonal matrices with elements:

$$\begin{pmatrix} -2 & 1 & 0 & \cdots & 1 \\ 1 & -2 & 1 & 0 & \\ & \ddots & \ddots & \ddots & \\ & 0 & 1 & -2 & 1 \\ 1 & & 0 & 1 & -2 \end{pmatrix}.$$

We observe that the matrices $D_{2,n}$, $D_{2,m}$ are obtained by computing the second order central difference operator with periodic condition in the horizontal and vertical directions [9].

In this case the linear system to be solved (7) is of the form:

$$(\mathbf{K}^T\mathbf{K} + \lambda\mathbf{L}^T\mathbf{L})\mathbf{f} = H^T\mathbf{g}. \tag{15}$$

In the deblurring applications, by assuming periodic boundary conditions, $\mathbf{K}$ is a Block Circulant matrix with Circulant Blocks (BCCB) [9]. Hence the coefficient matrix of the system (15) can be diagonalized by Unitary Discrete Fourier Transforms as follows:

$$\mathbf{K} = \mathbf{F}^* D\mathbf{F}, \quad \mathbf{D} = diag(d_1, \dots d_N), \quad \mathbf{L} = \mathbf{F}^* M\mathbf{F}, \quad M = diag(\mu_1, \dots \mu_N),$$

where $N = n \cdot m$, so that

$$\mathbf{f} = \mathbf{F}^*\Phi(\lambda)\mathbf{F}\mathbf{g}, \quad \Phi(\lambda) = \frac{|d_\ell^2|}{|d_\ell|^2 + \lambda|\mu_\ell|^2}. \tag{16}$$

The solution $\mathbf{f}$ for a given value λ requires 4 bidimensional Fast Fourier Transforms applied to the $n \times m$ image.

3 Experimental Results

In this section we present some results to show the effectiveness of the proposed method in different application problems. The numerical tests have been performed using matlab on AMD Athlon 64 processor with 2.01 GHz and 2 GB ram. The matlab codes can be downloaded from the authors' web pages (url `http://www.dm.unibo.it/~piccolom, http://www.dm.unibo.it/~zama`). We show several results obtained by applying the `CLSRit` algorithm, with $k_s = 2$, to solve the problem (3) in different application areas. In particular we analyze the following cases:

- $\mathbf{K} = I$ (paragraph 3.1). Image denoising problem with Total Variation function as regularization operator: $\mathcal{R}(\mathbf{f}) = TV(\mathbf{f})$ (13).
- $\mathbf{K} \neq I$:
  - Image Deblurring (paragraph 3.2). In this case $\mathbf{K}$ is the discrete convolution operator and the regularization operator $\mathcal{R}$ is the 2-norm i.e.$\mathcal{R}(\mathbf{f}) = \|\nabla^2(\mathbf{f})\|_2$
  - Image reconstruction from projections (paragraph 3.3). In this case $\mathbf{K}$ is the discrete tomographic operator and the regularization operator $\mathcal{R}$ is the Total Variation function :$\mathcal{R}(\mathbf{f}) = TV(\mathbf{f})$ (13).

3.1 Image Denoising Experiment

This experiment consists in removing additive noise from an image by solving problem (3). In the example reported in table 2 noisy test images $\mathbf{g}^\delta$ are obtained

by adding to the original image $\mathbf{f}_{true}$ (figure 1(a)) a noise image $\delta \cdot \eta$ where η is a random image such that $\|\eta\|_F = 1$ and the scalar δ is such that:

$$\frac{\|\mathbf{g}^\delta - \mathbf{f}_{true}\|_F}{\|\mathbf{f}_{true}\|_F} = \delta, \tag{17}$$

where $\|\cdot\|_F$ is the Frobenius norm. The results are obtained by adding different amount of noise and applying the `CLSRit` algorithm with $\mathcal{R}(\mathbf{f}) = TV(\mathbf{f})$. The comparison between the original and the noisy image, as well as the original and computed image, is performed by the following error parameters:

- the Relative Error (RE):

$$RE = \frac{\|\mathbf{f}_{true} - \mathbf{f}\|_F}{\|\mathbf{f}_{true}\|_F,} \quad SNR = 20log_{10}RE^{-1}$$

- the Structural Similarity Index in Image Space (SSIM) used to define the image structural similarity [6]. This parameter is evaluated using the matlab function `ssim.m` given in url `http://www.ece.uwaterloo.ca/~z70wang/research/ssim/`. The optimal value is $SSIM = 1$ and is relative to the case $RE = 0$.

The data reported in table 2 show the results obtained with noise level δ in the range $[5 \cdot 10^{-2}, 5 \cdot 10^{-1}]$ with SNR in the range $[6, 26]$. The improvement in the image quality is evident in the increase of the SNR value that is in the range $[17, 29]$ after the denoising process. The values of the SSIM parameter are larger with respect to the noisy image and closer to the optimal value 1.

In column 4-th are reported the iterations k of the hybrid method to compute the succession λ_k and the total number of iterations performed by the solver of the inner nonlinear system (7). In this case the Fixed Point method with Conjugate Gradient (CG) method is used [5], so the value it is relative to the Conjugate Gradient iterations. In this problem γ is computed as in (12) with $\gamma_L \equiv \mathcal{R}(\mathbf{f}_L)$ where $\mathbf{f}_L$ is obtained by a gaussian low pass filter with variance equal to 20% of the image power spectrum and the value γ_H is obtained by the noisy data $\gamma_H \equiv \mathcal{R}(\mathbf{g})$. The value $\theta = 0.5$ is used unless otherwise indicated.

In figure 2(a) the sequence λ_k is reported showing as triangle the value computed by the algorithm and as dot the value relative to the minimum relative error in the case $\delta = 0.2$. In this case the number of iterations k is slightly larger than the optimal one, but it does not give a significant increase in the relative error (figure 2(b)). The plots of $\mathcal{R}(\mathbf{f})$ vs. γ reported in figure 2(c) shows that few iterations are required for the convergence of the sequence $\{\lambda_k\}$. Finally the quality of the computed solutions can be evaluated by figures 1(c) and 1(d) representing a zoom of the same detail from the noisy image and the image reconstructed by the `CLSRit` method.

3.2 Image Deblurring Experiment

In this paragraph we present the numerical results obtained with the proposed algorithm when $\mathbf{K}$ is the discrete convolution operator and the regularization

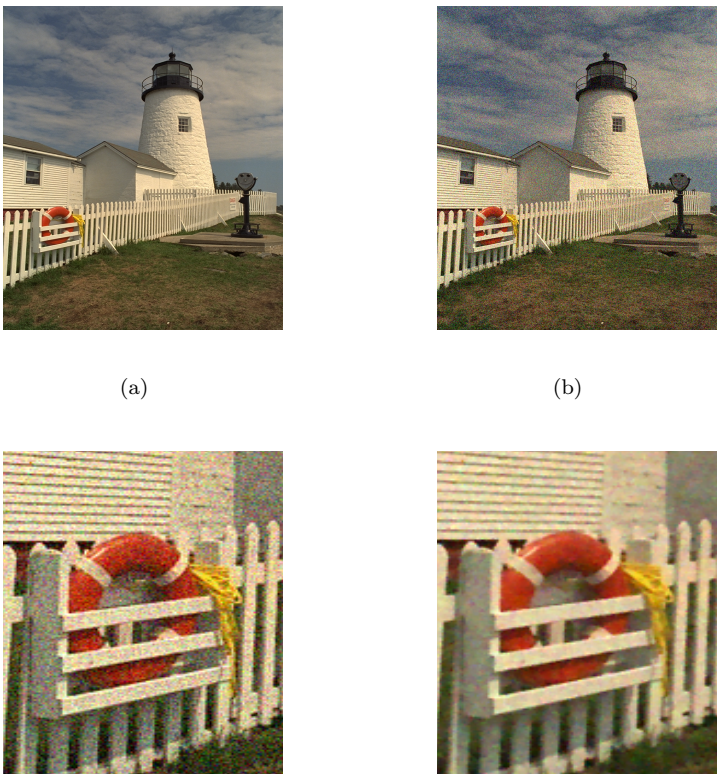

(a) (b)

(c) (d)

Figure 1: Denoising Test. (a) Original 768×512 true color image.(b) Noisy Image $\delta = 0.2$, $SNR = 14.98$; (c)Detail of the noisy image (d) Detail of the reconstructed image ($RE = 6.509e - 2$, $SNR = 23.73$)

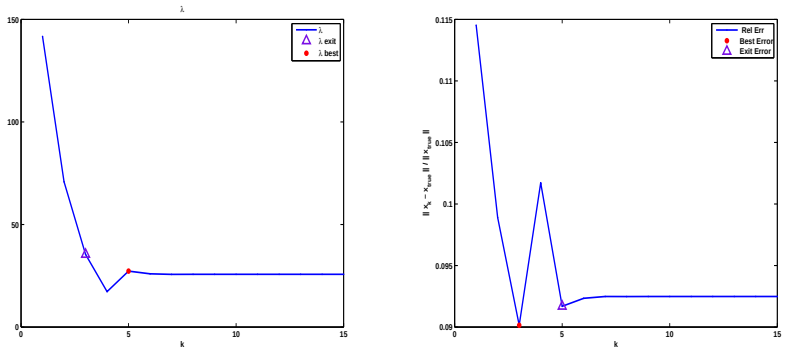

(a) (b)

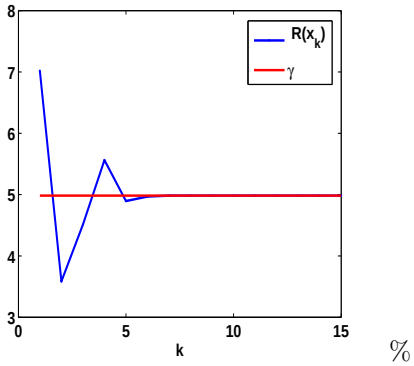

(c)

Figure 2: Denoising Test: case $\delta = 0.2$. (a) Succession λ_k (b) Relative error; (c) $R(x_k)$ and γ

Noisy Image Errors			Iterations	Computed Image Errors			γ
δ	SNR	SSIM	k(it)	RE	SNR	SSIM	
5e-2	26	9.755e-1	8(302)	3.678e-2	29	9.827e-01	4.801 $^{(1)}$
1e-1	20	9.127e-1	5(199)	6.509e-2	28	9.539e-1	4.155
2e-1	14	7.502e-1	5(196)	9.169e-2	21	8.609e-1	4.983
5e-1	6	4.196e-1	3(160)	1.439e-1	17	7.329e-1	3.044 $^{(2)}$

Table 2: Image Denoising Experiment. $\mathcal{R}(\mathbf{f}_{true}) = 4.96$, $^{(1)}$ $\theta = 0.2$; $^{(2)}$ $\theta = 0.6$

operator $\mathcal{R}$ is the 2-norm of the discrete Laplacian operator applied to the image $\mathbf{f}$:

$$\mathcal{R}(\mathbf{f}) = \|\nabla^2(\mathbf{f})\|_2$$

The 256×256 test image, shown in figure 3, is blurred using both gaussian and motion blur Point Spread Functions (PSF) obtained from Matlab Image Processing Toolbox (IPT) function `fspecial` as follows:

- Gaussian blur with parameters $\texttt{Hsize} = 11, \texttt{sigma} = 2$: `PSF=fspecial('gaussian',Hsize,sigma);`.
- Motion blur with parameters $\texttt{Len} = 10, \texttt{Theta} = 45$: `PSF=fspecial('motion',Len,Theta);`

The blurred images $\mathbf{g}$ are obtained by convolution of the given image $\mathbf{f}_{true}$ and the Point Spread Functions `PSF` using the IPT Matlab function `imfilter`:

$$\mathbf{g} = \texttt{imfilter}(\mathbf{f}_{\texttt{true}}, \texttt{PSF}, '\texttt{symmetric}').$$

The blurred noisy images $\mathbf{g}^\delta$ are obtained by adding to the blurred image $\mathbf{g}$ a noise image $\delta \cdot \underline{\eta}$ s.t.:

$$\frac{\|\mathbf{g}^\delta - \mathbf{g}\|_F}{\|\mathbf{g}\|_F} = \delta.$$

The experiment consists in solving problem (3) with noise values δ given by $1 \cdot 10^{-2}, 5 \cdot 10^{-2}, 1 \cdot 10^{-1}$ (figures 4(a) and 4(c) show the case $\delta = 1 \cdot 10^{-1}$ with gaussian and motion blur respectively). In tables 3 and 4 are reported the results obtained in the case of gaussian blur and motion blur respectively. The percentage of blur error with respect to the total error is measured by the parameter NP:

$$NP = 100 \frac{\|\mathbf{g} - \mathbf{f}_{true}\|_F}{\|\mathbf{g}^\delta - \mathbf{f}_{true}\|_F}$$

in our experiments the amount of blur is 77 - 99 of the total error and the SNR is in the range $[14, 19]$. The number of iterations k required by the algorithm reported in column 3 of tables 3 and 4 is in the range $[3, 16]$, showing fast convergence of the sequence λ_k and high computational efficiency. Indeed, the total computational cost is $(3 + k)FFT2(n, m)$ where k is the number of iterations

(always < 20) and $FFT2(n, m)$ is the bidimensional Fast Fourier Transform of the $n \times m$ test image (in our example $n = m = 256$). The quality of the restored images can be appreciated by the increased SNR value, (table 4 column 6−th) and by figures 4(b) and 4(d) relative to the cases $RE(\mathbf{g}^\delta) = 1.174e-1$ (gaussian blur) and $RE(\mathbf{g}^\delta) = 1.851e-1$ (motion blur).

In figures 5 and 6 are represented the relative error depending on the value of the parameter γ in (3). The error curves (RE) relative to two different noise values $\delta = 1.174e-1$ and $\delta = 1.517e-1$ (table 3) are obtained by running the algorithm with different values of the parameter γ in the range $[1.e-5, 1.e-2]$ (figure 5). We observe that the value $\gamma_{true} \equiv \mathcal{R}(\mathbf{f}_{true})$ does not give the minimum RE and that the optimal value becomes smaller by increasing the noise level. Furthermore we see that the values of γ computed by the algorithm (plotted with triangles and dots) are very close to the optimal. Figures 6 show the effectiveness of the technique used for computing the values γ_L and γ_H s.t. $\gamma_L < \gamma < \gamma_H$. In this problem $\gamma_L \equiv \mathcal{R}(\mathbf{f}_L)$ where $\mathbf{f}_L$ is obtained by Wiener filtering the data $\mathbf{g}^\delta$ with parameter

$$W = \min_\ell \left| \frac{(\mathbf{F}\mathbf{g}^\delta)_\ell}{d_\ell} \right|$$

where $\mathbf{K} = \mathbf{F}^*\mathbf{D}\mathbf{F}$, $\mathbf{D} = diag(d_\ell)$ as in (16). The value γ_H is set as $10\gamma_L$ and γ is computed by (12) with $\theta = 0.5$. We observe that the minimum relative error is always included in the interval $[\gamma_L, \gamma_H]$.

Blurred Noisy Image Errors			Iterations	Computed Image Errors		γ
δ	NP	SNR	k	RE	SNR	
1.174e-1	99.7	19	16	5.059e-2	26	3.540e-4
1.266e-1	92.4	18	15	7.793e-2	20	3.875e-3
1.517e-1	77.2	16	14	9.466e-2	22	3.110e-3

Table 3: Gaussian Blur and Gaussian Noise $\mathcal{R}(\mathbf{f}_{true}) = 6.206e-03$, $\theta = 0.5$

Blurred Noisy Image Errors			Iterations	Computed Image Errors		γ
δ	NP	SNR	k(it)	RE	SNR	
1.851e-1	99.9	15	6	5.74e-2	25	2.822e-3
1.911e-1	96.7	14	10	9.76e-2	20	1.530e-3
2.085e-1	88.7	14	3	1.25e-1	18	1.351e-3

Table 4: Motion Blur and Gaussian Noise $\mathcal{R}(\mathbf{f}_{true}) = 6.206e-03$, $\theta = 0.5$;

3.3 Tomographic Reconstruction Experiment

In this paragraph we report some results of tomographic reconstruction experiment. The data $\mathbf{g}$, representing the response of a fan beam RX tomographic

Figure 3: Image Deblurring test image (256×256 pixels).

detector, are vectors of $P \cdot N\theta$ elements, where P is the number of projection rays and $N\theta$ is the number of projection angles in the range $[0, 2\pi]$. The original image, shown in figure 3.3, is the $N \times N$ pixels Shep-Logan phantom and the synogram $\mathbf{g}$ is generated by the matlab function `fanbeam.m` by J. H.Jorgensen, M. S. Hansen and P. C. Hansen, available at the url http: //www2.imm.dtu.dk/ pch/ TVReg/index.html. The results reported in table 5 are relative to the case $N = 512$, $P = 724$, $N\theta = 360$. The noisy data $\mathbf{g}^\delta$ are obtained by adding to the synogram y a noise vector $\delta \cdot \underline{\eta}$ where $\underline{\eta}$ is a random vector such that $\|\underline{\eta}\|_2 = 1$ and the scalar δ is such that:

$$\frac{\|\mathbf{g}^\delta - \mathbf{g}\|_2}{\|\mathbf{g}\|_2} = \delta.$$

The value γ is computed as in (12) where $\gamma_L = \mathcal{R}(\mathbf{f}_L)$ is is computed by applying few (< 5) iterations of the CG method applied to the normal equation system: $\mathbf{K}^T\mathbf{K}\mathbf{f} = \mathbf{K}^T\mathbf{g}^\delta$ and the value $\gamma_H = 10 \cdot \gamma_L$.

The inner minimization problem (14) is solved by means of the Two-Step Iterative Shrinkage/Thresholding Algorithm (TWIST) [3] and the total number of inner iterations are reported in table 5 column 3−rd. In column 2 and 5 is reported the SNR with respect to the noisy synogram $\mathbf{g}^\delta$ and the synogram obtained by the reconstructed image: $\mathbf{g}_k = \mathbf{K}\mathbf{f}_k$. Also in this case we observe fast convergence of the λ_k sequence (< 20 iterations) and the improvement in the quality of the reconstruction (figures 8(a) and 8(b)). Finally in figure 8(c) we observe that the exit iteration is close to the optimal without a substantial increase of the relative error.

4 Conclusions

In this work we have extended to imaging applications a method that we proposed in [1] for the solution of a regularization problem and the computation of

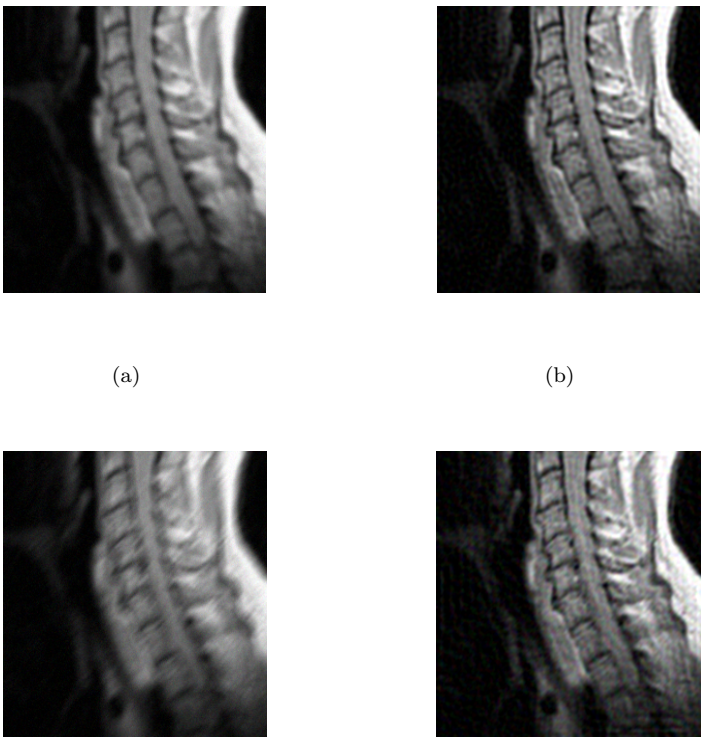

(a) (b)

(c) (d)

Figure 4: Deblurring Test problem. (a) Noisy gaussian blurred $\delta = 1.266e-1$, $SNR = 18$; (b) Restored Image $SNR = 20$ (c) Noisy motion blurred $\delta = 1.911e-1$, $SNR = 14$ (d) Restored image $SNR = 20$

the regularization parameter by giving an estimate of the regularity required on the solution. We have implemented the method with the regularization functions mainly used in inverse imaging, i.e. the Tikhonov and the Total Variation. The numerical tests performed in image denoising, deblurring and tomographic reconstruction show that the iterative method proposed is computationally efficient for large size problems, since few external iterations are needed to compute a good value of the parameter. In future work, the method could be extended to the case of a fully nonlinear objective function, where the fit-to-function could be, for example, the Kullback-Leibler (or Csiszàr I-divergence).

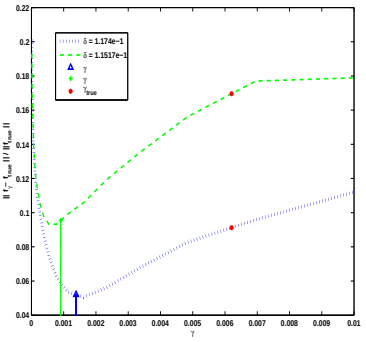

Figure 5: Relative error vs γ with two noise levels: $\delta = 1.174e{-}1$, $\delta = 1.517e{-}1$.

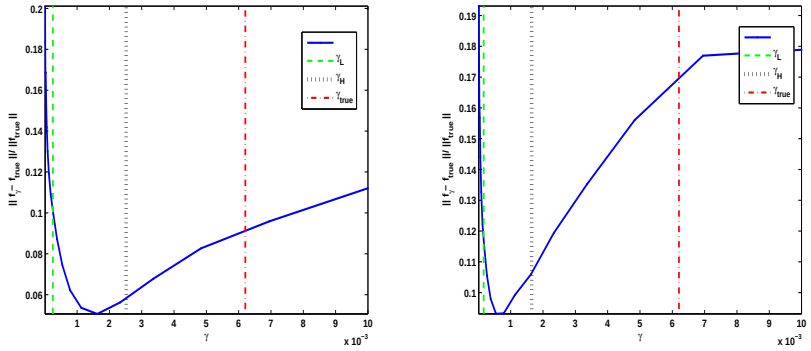

(a) (b)

Figure 6: Values γ_L (green dash line), γ_H(black dot line) and γ_{true} (red dash dot line), used for computing γ (a) $\delta = 1.174e-1$, (b) $\delta = 1.517e-1$

Figure 7: Shepp Logan Phantom 512×512 pixels.

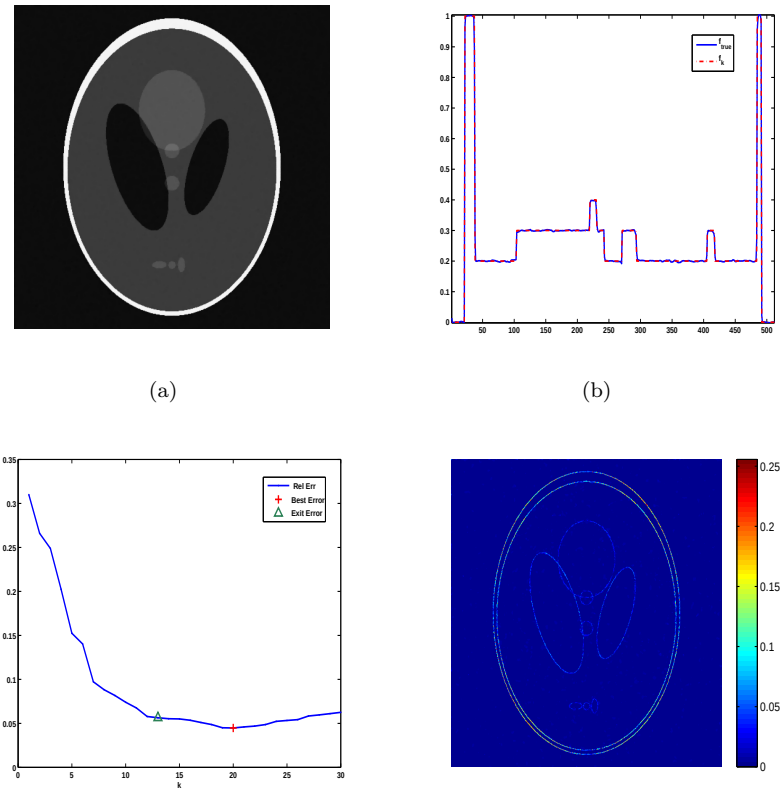

(a) (b)

(c) (d)

Figure 8: Tomography test problem. (a) Reconstructed Image $\delta = 1.e-2$, $SNR = 46$; (b) Row 256 original (red dashed) and reconstructed image (blue line) (c) Relative error vs. iterations. Green triangle: exit of the algorithm; Red +: best error. (d) Difference Image;

Noisy Synogram δ	SNR $\mathbf{g}^\delta$	Iterations k(it)	Reconstructed Image Errors RE	SNR $\mathbf{g}_k$	SSIM	γ
1e-2	40	17(783)	8.584e-2	44.2	9.83e-1	9.0e+3
		13(582)	5.060e-2	46.8	9.95e-1	5.318e+3 (1)
1e-1	20	18(363)	1.342e-1	33.6	8.810e-1	4.421e+3

Table 5: Tomographic Image Recostruction $\mathcal{R}(\mathbf{f}_{true}) = 2.928e + 3$. (1) $\theta = 0.2$;

5 Acknowledgments

This work was supported by the MIUR grant number 2008T5KA4L.

References

[1] E. Loli Piccolomini, F. Zama An iterative algorithm for large size least-squares constrained regularization problems. *Appl. Math. Comp.*, 217:10343-10354, 2011.

[2] I. Csiszár. Why least squares and maximum entropy? An axiomatic approach to inference for linear inverse problems. *Ann. Statist.*, 19:2032–2066, 1991.

[3] J. Bioucas-Dias and M. Figueiredo, A New TwIST: Two-Step Iterative Shrinkage/Thresholding Algorithms for Image Restoration. *IEEE Transactions on Image processing*, 2007.

[4] H. W. Engl and M. Hanke and A. Neubauer Regularization of Inverse Problems Kluwer Academic Publishers,1996

[5] C. R. Vogel and M. E. Oman, Iterative methods for total variation denoising, *SIAM J. Sci. Comput.*, 17:227-238, 1996

[6] Z. Wang and A. C. Bovik and H. R. Sheikh and E. P. Simoncelli Image Quality Assessment: From Error Visibility to Structural Similarity. *IEEE TRANSACTIONS ON IMAGE PROCESSING*, VOL. 13, NO. 4, 2004.

[7] P.C.Hansen, Regularization Tools: A Matlab package for analysis and solution of discrete ill–posed problems, *Numeric. Algor.*,VOL. 6,1:35,1994

[8] J. Dahl and P. C. Hansen and S. Jensen and T. Jensen Algorithms and software for total variation image reconstruction via first-order methods. *Numerical Alg.*, VOL. 53,67:92,2010

[9] P. C. Hansen, J. Nagy, and D. P. O'Leary. *Deblurring images. Matrices, Spectra and Filtering.* SIAM, 2006.

[10] R. Acar and R. C. Vogel, Analysis of Total variation penalty methods for ill-posed problems, Inv. Prob.,VOL. 10,1217:1229,1994.

[11] , A. N. Tikhonov, V. Y. Arsenin, *Solutions of Ill–Posed Problems*, *John Wiley & Sons*,1977

[12] C.R. Vogel and M.E. Oman, Fast, robust total variation–based reconstruction of noisy, blurred images, *IEEE Trans. on Image Processing*, VOL. 7,813:824,1998.

[13] C. R. Vogel, Computational Methods for Inverse Problems *SIAM*,2002

[14] P.C. Hansen, J. G. Nagy, and D. P. O'Leary, *Deblurring Images, Matrices, Spectra and Filtering*, SIAM, 2006.